Letters in Applied NanoBioScience
Open-Access Journal (ISSN: 2284-6808)

Article
Volume 15, Issue 2, 2026, 80
https://doi.org/10.33263/LIANBS152.080

Molecular Docking, Dynamics, and MM/GBSA-based Evaluation of Antidiabetic Phytoconstituents from *Pterocarpus marsupium*

Siddhi Tambe [1], Vishnu Choudhari [1], Rohini Pujari [1,*], Vrushali Tambe [2], Anita Malusare [2]

[1] School of Health Sciences and Technology, Dr. Vishwanath Karad MIT World Peace University, Kothrud, Pune-411038, Maharashtra, India
[2] Department of Pharmaceutical Chemistry, Progressive Education Society's Modern College of Pharmacy, Moshi, Pune, Maharashtra - 412105, India
* Correspondence: rohini.pujari@mitwpu.edu.in;

Received: 19.03.2025; Accepted: 15.02.2026; Published: 30.06.2026

Abstract: *Pterocarpus marsupium* Linn bark extract has been extensively used to treat Diabetes mellitus in Ayurveda. Given the traditional claim, this study was initiated to evaluate the antidiabetic potential of the phytoconstituents in the heartwood and bark by examining their binding to targets such as Sodium glucose cotransporter-2, Dipeptidyl peptidase-4, AMP-activated protein kinase, and Aldose reductase. The docking studies were carried out using PyRx and AutoDock Vina 1.1.2 software. The binding affinities of Pteroside with Sodium glucose co-transporter-2 (-9.5 Kcal/mol), 7-O-α-L-rhamnopyranosyloxy-4′-methoxy-5-hydroxy isoflavone with Dipeptidyl peptidase-4 (-8.9 Kcal/mol), and with AMP-activated protein kinase (-8.7 Kcal/mol), and Vijayoside with Aldose reductase (-9.1 Kcal/mol) were maximum as compared to the reference cocrystallized ligand. Molecular dynamics simulation studies indicate stable binding throughout the 100 ns simulation. MM-GBSA analysis elucidated the thermodynamic profile of the binding process and highlighted the key interactions governing complex stability. Among the evaluated complexes, Pteroside consistently demonstrated the strongest interaction profile with sodium glucose cotransporter-2. In view of this, clinical studies are necessary to elucidate their roles in the treatment of diabetes mellitus.

Keywords: *Pterocarpus marsupium*; molecular dynamics simulation; SGLT-2; DPP-4; aldose reductase; AMPK; antidiabetic.

1. Introduction

Diabetes mellitus (DM) is an ailment of priority research to the scientific community all over the globe. DM can be classified into type 1 and type 2, characterized by irregular glucose homeostasis. Sodium glucose cotransporter-2 (SGLT-2), Dipeptidyl Peptidase-4 (DPP-4), AMP-activated protein kinase (AMPK), and Aldose reductase (AR) are already established targets for DM. SGLT-2 is a protein prominently expressed in the kidneys. It is responsible for 90% of renal glucose reabsorption. In type 2 DM, inhibition of SGLT-2 results in glucose excretion [1]. Gliflozin is an anti-diabetic drug class acting as an SGLT-2 inhibitor [2]. DDP-4 is a serine exopeptidase that can inactivate various oligopeptides by removing N-

terminal dipeptides. Incretin hormones regulate the secretion of insulin after meals. Some type 2 DM patients exhibit incretin protein deficiency. Glucagon-like peptide 1 (GLP-1) and glucose-dependent insulinotropic polypeptide (GIP) are two major incretins secreted by the gastrointestinal tract. These suppress the secretion of glucagon while enhancing the secretion of insulin. During the normal metabolic process, DPP-4 removes incretin from the body. Hence, DPP-4 inhibitors are useful in type 2 DM [3]. Gliptins are competitive DPP-4 inhibitors [4]. AMPK is an alpha-beta-gamma heterotrimer that can sense cellular energy. It gets activated with a drop in energy levels. It stimulates the oxidation of fatty acids in adipose and other tissues, increases glucose uptake in skeletal muscles, and reduces glucose production in the liver [5]. A benzimidazole derivative was found to increase glucose transport in skeletal muscle. Metformin is reported to be an activator of AMPK, thereby increasing muscle glucose uptake [6]. Similarly, Diabetic complications, such as cataract, are mediated by Aldose reductase (AR) and advanced glycation end products (AGEs) [7]. AR, together with nicotinamide adenine dinucleotide phosphate, converts glucose to sorbitol. Sorbitol dehydrogenase further converts sorbitol to fructose. There is an accumulation of sorbitol in tissues due to poor sorbitol penetration and metabolism, giving rise to complications such as glaucoma and cataracts [8].

Pterocarpus marsupium (PM) Linn bark extract (Vijayasar) has been extensively used to treat DM in Ayurveda. Experimentally, Pterostilbene (PBS), a constituent of PM, has also shown its potency and efficacy against diabetic complications [9] and diabetic neuropathy [10]. Diabetic nephropathy is associated with AGE end products and oxidative stress. PBS decreased kidney lipid peroxides and nitrate levels along with a decrease in AGEs formation [11]. PBS may delay diabetic retinopathy progression by alleviating inflammation and suppressing the proliferation of human retinal endothelial cells [12]. Similarly, phenolic-C-glycosides in the heartwood are reported to have antihyperglycemic activity [13]. Additionally, (-) Epicatechin was found to increase insulin release due to increased cAMP content of the islets [14]. Still, there are limited reports exploring the role of other phytoconstituents of PM. Computational techniques can facilitate drug discovery through traditional claims. In the current study, molecular docking and molecular dynamics were employed to assess the potential of PM phytochemicals as inhibitors or stimulators of DM targets. The comparison with the reference ligands is also performed. The study is further extended to an ADMET (absorption, distribution, metabolism, excretion, and toxicity) drug-likeness study.

2. Materials and Methods

2.1. Selection of phytochemicals of PM.

A library of PM phytoconstituents was built from the Indian Medicinal Plants, Phytochemistry and Therapeutic (IMPPAT) database [15, 16] and systematic literature survey [13, 17-21]. The study aimed to arrive at the phytoconstituents of PM with Antidiabetic potential; hence, all reported phytoconstituents of the plant were selected. Their SDF formats were downloaded from Pubchem [22]. Avogadro 1.2 software [23, 24] and Autodock tools 1.5.7 (http://mgltools.scripps.edu) [25] were used to convert them into PDB and pdbqt format, respectively.

2.2. Selection of molecular targets and docking analysis.

The structures of proteins with cocrystallized ligand were retrieved from the RCSB Protein Data Bank (http://www.rcsb.org/), and their details are given in Table 1.

Table 1. Coordinates of grid boxes for molecular docking.

Receptor	PDB ID	Resolution	Coordinate (A^0)			Ligand (interacting Amino acids)	Ref
			X	Y	Z		
SGLT-2 Chain A	7VSI	2.95 Å	37.44	48.47	43.67	Empagliflozin (ASN-75, PHE-98, GLU-99, SER-287, LYS-321, GLN-457)	[26]
DPP-4 Chain A	4FFW	2.95 Å	19.54	-11.29	51.85	Sitagliptin (ARG-123, GLU-203, ARG-356 and TYR-663)	[27]
AMPK	4CFE	3.02 Å	478.56	42.06	989.01	Benzimidazole derivative (LYS-29 and ASP-88)	[28]
AR Chain A	2FZD	1.08 Å	15.85	5.34	15.03	Tolrestat (TRP-111, HIS-110, TYR-48, SER-302)	[29]

Further, AutoDock Tools was used for the preparation of proteins. From the protein structures, water molecules were removed. Hydrogen bond interactions between ligands and amino acids were facilitated by the addition of polar hydrogen atoms. Further steps involved the removal of heteroatoms, repair of missing atoms, addition of Kollman charges, building the molecule by distance, and assigning each atom an AD4 type. The position of the inhibitor or activator was considered as the location of the binding site. Virtual screening of selected targets was performed by blind molecular docking of phytochemicals onto the receptor centered about the active site by using PyRx (GUI version 0.8 of AutoDock) open-source software (https://pyrx.sourceforge.io) [30]. The docking analysis of the potential hits was repeated using AutoDock Vina 1.1.2 [25]. The grid box size as the search area was adjusted according to the size of the ligand. The grid size was 40 along all directions with a grid spacing of 0.375. The energy range was set at 4, and exhaustiveness was set at 8.0. The PDB files were converted into pdbqt format. Discovery Studio 3.5 Visualizer (https://discover.3ds.com) was used to visualize the saved poses. Comparison of scores of reference cocrystallized ligands with selected hits was done.

2.3. Drug likeliness study.

Drug effectiveness is determined by Pharmacokinetic parameters. They were predicted by using the SwissADME server [31]. The structures of the compounds were submitted to this server to predict the promising hits. The druglike nature of the selected ligands was studied on the basis of Lipinski's rules of five, water solubility, human gastrointestinal absorption capability, n-octanol and water (log Po/w) partition coefficient, and total polar surface area.

2.4. Molecular dynamics simulation (MDS).

The MDS study is performed to predict the stability of protein-ligand interactions based on changes in conformation over a timescale during dynamic-level interactions. The Desmond 2020.1 from Schrödinger, LLC was used to run MD simulations on docked complexes, viz. 2FZD_VIJ, 4CFE_RIF, 4FFW_RIF and 7VSI_PSD. The OPLS-2005 force [32] and explicit solvent model with the SPC water molecules were used [33] in a periodic boundary solvation box of 10 Å x 10 Å x 10 Å dimensions. Na^+ ions were added to neutralize the charge, followed by 0.15 M NaCl solutions to simulate the physiological environment. Initially, the system was equilibrated using an NVT ensemble for 10 ns to retrain over the protein-ligand complexes.

Following the previous step, a short run of equilibration and minimization was carried out using an NPT ensemble for 12 ns. This ensemble was set up using the Nose-Hoover chain coupling scheme [34] with varying temperatures, a relaxation time of 1.0 ps, and a pressure of 1 bar maintained in all simulations. A time step of 2fs was used. The Martyna-Tuckerman–Klein chain coupling scheme [34] barostat method was used for pressure control with a relaxation time of 2 ps. The particle mesh Ewald method was used for calculating long-range electrostatic interactions, and the radius for the Coulomb interactions was fixed at 9Å. The final production run was carried out for 100ns. The root-mean-square deviation (RMSD), radius of gyration (Rg), root-mean-square fluctuation (RMSF), and the numbers of hydrogen bonds, salt bridges, and SASA are calculated to monitor the stability of the MD simulations [32].

2.5. Binding free energy analysis.

The molecular mechanics combined with the generalized Born surface area (MM-GBSA) approach was used to compute the binding free energies of the ligand-protein complexes. The Prime MM-GBSA binding free energy was calculated using the Python script thermal mmgbsa.py in the simulation trajectory for the last 50 frames with a 1-step sampling size. The binding free energy was estimated using the principle of additivity, in which individual energy modules such as Coulombic, covalent, hydrogen bond, van der Waals, self-contact, lipophilic, protein solvation, and ligand were added. The following equation was used to calculate ΔG_{bind}:

$$\Delta G_{bind} = \Delta G_{MM} + \Delta G_{Solv} - \Delta G_{SA} \quad (1)$$

Where, ΔG_{bind} designates the binding free energy, ΔG_{MM} designates the difference between the free energies of ligand-protein complexes and the total energies of protein and ligand in isolated form, ΔG_{Solv} designates the difference in the GSA solvation energies of the ligand-receptor complex and the sum of the solvation energies of the receptor and the ligand in the unbound state, ΔG_{SA} designates the difference in the surface area energies for the protein and the ligand [32].

3. Results and Discussion

A series of computational techniques was used to identify the most promising natural compound analog from PM as an antidiabetic agent, namely PyRx, AutoDock Vina, and MDS. The library of phytoconstituents of PM (Table 2) was screened through a molecular docking-based virtual screening method using PyRx. The comparative status of binding interactions of all phytoconstituents obtained using PyRx is given in Table 3. The results of drug likeness and ADMET parameters are given in Table 4. The top five scoring ligands with stable binding to selected receptors obtained by PyRx were further studied using AutoDock Vina.

Table 2. Structures of selected compounds used for docking.

Ligand	Structure	Ligand	Structure
Pteroside	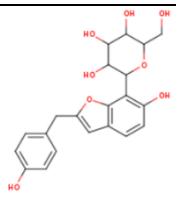	7-O-α-L-rhamnopyranosyloxy-4′-methoxy-5-hydroxy isoflavone	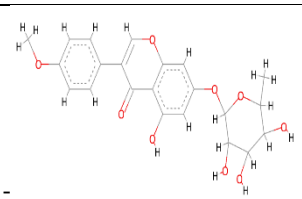

Ligand	Structure	Ligand	Structure
Naringetol	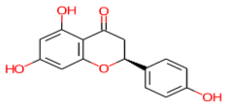	Pseudobaptigenin	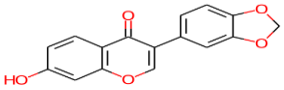
3,7,4'-Trihydroxyflavone	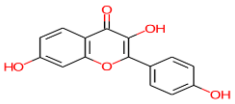	7,4'-Dihydroxyflavone	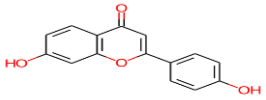
Liquiritigenin	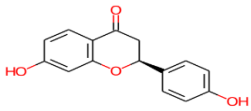	(2S)-7-hydroxyflavanone	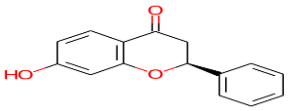
Isoliquiritigenin	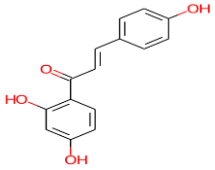	Oleanolic acid	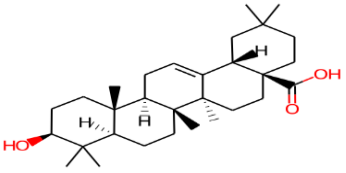
Lupeol	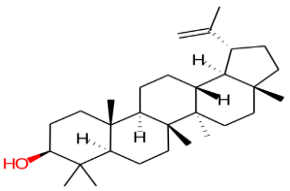	Pterostillbene	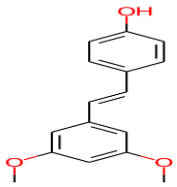
Propterol	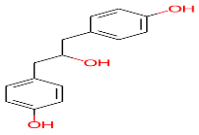	5-de-oxykaempferol	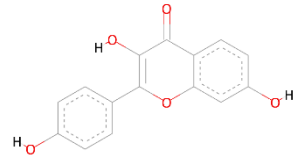
Beta-eudesmol	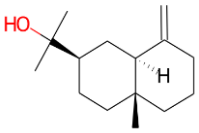	Vijayoside	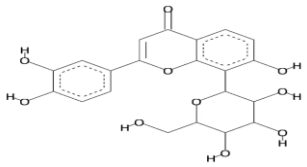
Pterosupin	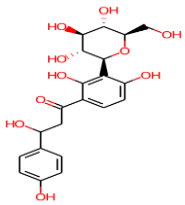	Trans-Stilbene	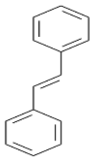
Epicatechin	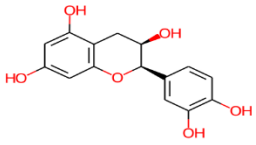	Garbanzol	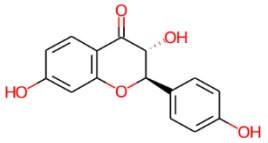
Marsupium	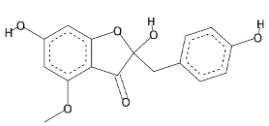	Marsupol	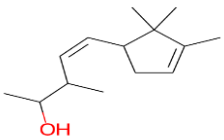
Gallic acid	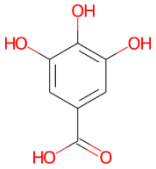	3,4-Dihydroxybenzoic acid	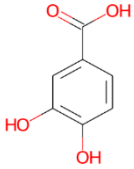

Ligand	Structure	Ligand	Structure
4-hydroxybenzaldehyde	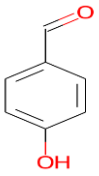	Catechol	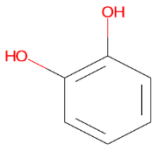

Table 3. List of phytoconstituents of PM with binding energy (PyRx) with different targets.

Sodium glucose co-transporter 2 (7VSI)		Dipeptidyl peptidase (4FFW)		AMPK (4CFE)		Aldose reductase (2FZD)	
Ligand	**BA**	**Ligand**	**BA**	**Ligand**	**BA**	**Ligand**	**BA**
PSD	-10.1	Oleanolic acid	-9.4	Oleanolic acid	-10	Lupeol	-9.1
RIF	-9.9	Lupeol	-9	DHF	-9.5	VIJ	-9.1
Naringetol	-9.8	RIF	-9	PSD	-9.5	HF	-9
Pseudobaptigenin	-9.3	Pseudobaptigenin	-8.1	DOK	-9.4	DHF	-9
THF	-9.2	PSD	-7.9	Pseudobaptigenin	-9.2	RIF	-9
DHF	-9.1	Epicatechin	-7.9	HF	-9	Oleanolic acid	-8.9
Liquiritigenin	-9.1	VIJ	-7.8	Naringetol	-9	PSD	-8.6
HF	-9	Naringetol	-7.4	RIF	-9	Liquiritigenin	-8.4
Isoliquiritigenin	-9	Pterosupin	-7.4	Garbanzol	-8.9	Pseudobaptigenin	-8.4
Oleanolic acid	-9	DHF	-7.3	Lupeol	-8.9	Epicatechin	-8.4
Lupeol	-8.8	Garbanzol	-7.3	Pterosupin	-8.8	THF	-8.3
Pterostillbene	-8.4	HF	-7.2	Marsupium	-8.6	DOK	-8.3
Propterol	-8.3	THF	-7.2	THF	-8.5	Naringetol	-8.3
DOK	-8.2	DOK	-7.2	Liquiritigenin	-8.5	Pterosupin	-8.3
Beta-eudesmol	-8.2	Liquiritigenin	-7.2	Isoliquiritigenin	-8.5	Propterol	-8.3
Vijayoside	-8.1	Beta-eudesmol	-7.2	Epicatechin	-8.4	Garbanzol	-8.3
Pterosupin	-7.9	Marsupium	-7.1	VIJ	-8.4	trans-Stilbene	-8.3
Trans-Stilbene	-7.8	Isoliquiritigenin	-7	Propterol	-8.3	Isoliquiritigenin	-7.6
Epicatechin	-7.5	Trans-stilbene	-6.9	Trans-Stilbene	-7.6	Marsupium	-7.5
Garbanzol	-7.5	Pterostillbene	-6.7	Pterostillbene	-7.4	Beta-eudesmol	-7.4
Marsupium	-7.4	Propterol	-6.5	Beta-eudesmol	-7.1	Pterostillbene	-7.4
Marsupol	-7.2	Marsupol	-5.9	Marsupol	-6.4	Marsupol	-6.9
Gallic acid	-7.1	Gallic acid	-5.8	DHB	-6.2	DHB	-5.7
DHB	-6.8	DHB	-5.6	Gallic acid	-6.1	Catechol	-5.7
HB	-6.1	HB	-5.3	HB	-5.4	Gallic acid	-5.7
Catechol	-5.8	Catechol	-5	Catechol	-5.1	HB	-5.4

BA: Binding energy in Kcal/mole; PSD: Pteroside; RIF: 7-O-α-L-rhamnopyranosyloxy-4′-methoxy-5-hydroxy isoflavone; HF: (2S)-7-hydroxyflavanone; HB: 4-hydroxybenzaldehyde; DHB: 3,4-Dihydroxybenzoic acid; DHF: 7,4'-Dihydroxyflavone; THF: 3,7,4'-Trihydroxyflavone; DOK: 5-de-oxykaempferol.

Table 4. Drug likelihood parameters.

Parameter (ideal values)	RIF	VIJ	PSD
Molecular formula	$C_{15}H_{10}O_2$	$C_{21}H_{20}O_{10}$	$C_{21}H_{22}O_8$
Molecular Weight (g/mol) (<500)	222.24	432.38	402.39
No. of H-bond acceptors (<10)	2	10	8
No. of H-bond donors (<5)	0	7	6
Log P o/w (iLOGP) (≤ 5)	2.51	1.10	1.83
Lipinski Violation (≤ 1)	0 violation	Yes; 1 violation: NHorOH>5	Yes; 1 violation: NHorOH>5
Molar Refractivity	67.92	106.61	102.33
Bioavailability Score	0.55	0.55	0.55
Topological polar surface area Å (≤ 140)	30.21	181.05	143.75
Number of rotatable bonds (≤ 10)	1	3	4

3.1. Molecular docking using AutoDock Vina.

3.1.1. Sodium glucose co-transporter 2 (7VSI).

Pteroside was found to bind more stably with SGLT-2 with a binding energy of -9.5 Kcal/mol. Similarly, 7-O-α-L-rhamnopyranosyloxy-4′-methoxy-5-hydroxy isoflavone (RIF, -9 Kcal/mol), 3,7,4'-Trihydroxyflavone (-8.2 Kcal/mol) were found to have more stable interactions as compared to Empagliflozin (-7.3 Kcal/mol). The binding energy of Naringetol and Pseudobaptigenin was found to be -7.6 and -6.8 Kcal/mol, respectively. Pteroside and the marketed drug Empagliflozin were found to dock at a similar site. The docking site and interactions of Pteroside are shown in Figure 1. Pteroside has formed CHB through GLU99, SER91, and THR87. Various other amino acids involved in the interaction are HIS80, PHE98 (PP), LEU84, VAL95 through PS interactions, while ASP454 (PA), and LEU274 (PAL) also showed interactions with the protein. It has been found to have two common interactions, such as that of ligand Empagliflozin (PHE-98, GLU-99). As the binding energy with Pteroside was minimum, it was further considered for MD simulation studies.

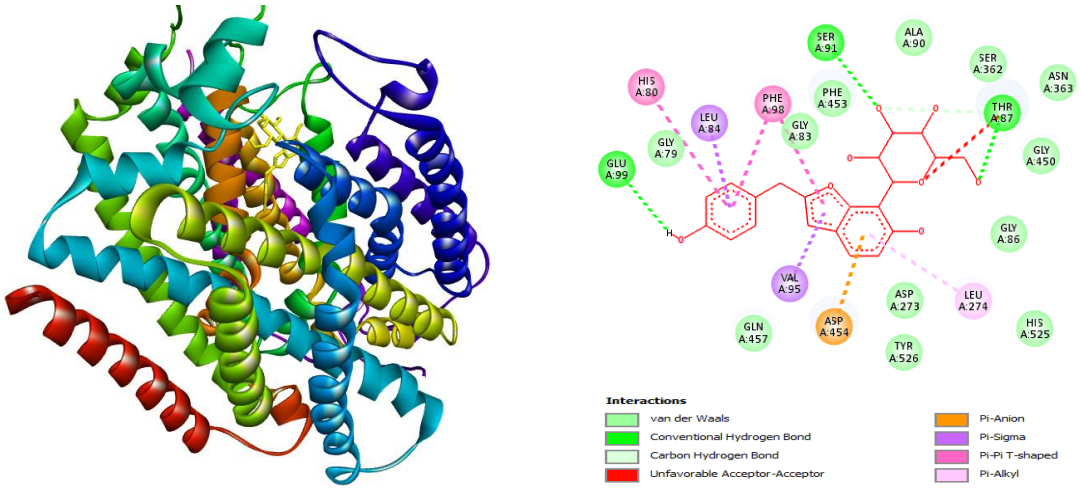

(a) **(b)**

Figure 1. (a) Docked pose of Pteroside (yellow) in the binding pocket of Sodium glucose co-transporter 2 (7VSI); **(b)** Interactions with Pteroside.

3.1.2. Dipeptidyl peptidase (DDP-4)/adenosine deaminase binding protein (4FFW).

The binding energy of RIF, Oleanolic acid, Lupeol, Epicatechin, Pteroside, Sitagliptin, and Pseudobaptigenin was found to be -8.9, -8.6, -8.6, -8.6, -8.3, -7.8, and -7.5 Kcal/mol, respectively. Compared with Sitagliptin, RIF, Oleanolic acid, lupeol, epicatechin, and pteroside were found to have more favorable binding energies. Interactions of RIF involved GLU204, ARG356, TYR663, and ASN711 (2 bonds) through CHB. PHE855 has formed two Pi-Pi staking interactions with rings of RIF. It was also found to interact with the carbon-hydrogen bond via SER631. It was found to have involvement of ARG-356 and TYR-663 residues in protein binding, as with ligand sitagliptin. PSD interacted through ILE372, ARG352 (CHB), ILE408, ALA358, ILE372 (PAL), GLU359 (PA), ARG354 (PC) and ARG354 (UDD). PSD and Sitagliptin were docked in the same cavity. The docking site of RIF and its interactions are shown in Figure 2. RIF was further considered for MD analysis.

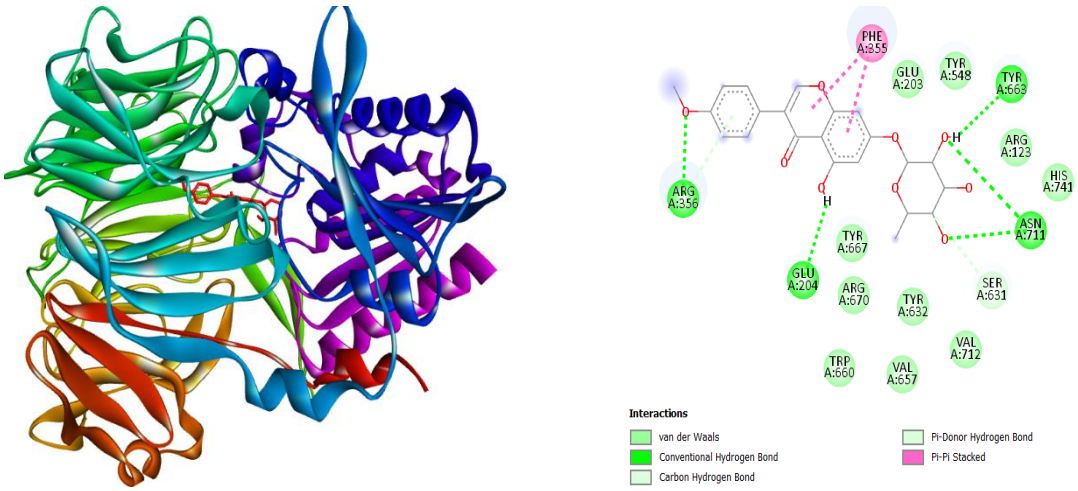

(a) **(b)**

Figure 2. (a) Docked pose of RIF(Red) in the binding pocket of DPP-4 (4FFW); **(b)** Interaction with RIF.

3.1.3. AMPK (4CFE).

The binding energies of RIF, DOK, 7,4'-Dihydroxyflavone, Pseudobaptigenin, Pteroside, oleanolic acid, and Benzimidazole derivative were found to be -8.7, -8.5, -8.4, -8.4, -7.6, -7.3, and -8.3 Kcal/mol, respectively. The binding pose of RIF is shown in Figure 3. It was found to interact majorly through VAL30, LEU146, LEU22, ALA43, and MET93. As the binding energy of RIF was found to be minimal, it was further considered for MD studies.

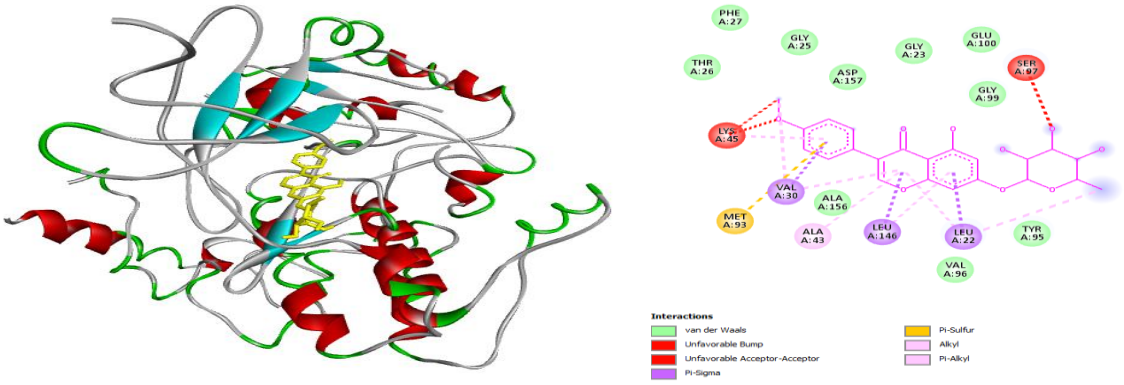

(a) **(b)**

Figure 3. (a) Docked pose of RIF (yellow) in the binding pocket of AMPK (4CFE); **(b)** Interaction with RIF.

3.1.4. Aldose reductase (2FZD).

Vijayoside was found to have maximum affinity for AR as per PyRx and AutoDock Vina scores. The binding energy of Vijayoside, (2S)-7-hydroxyflavanone, 7,4'-Dihydroxyflavone, RIF, Lupeol, and Tolrestat was found to be -9.1, -9.1, -9, -8.8, -8.3, and -7.5 Kcal/mol, respectively. The position of Vijayoside in the binding pocket is shown in Figure 4. All selected phytoconstituents were found to form stable interactions with the receptor as compared to Tolrestat. The binding of the most stable conformer of VIJ involved TRP20 (CHB), VAL47, HIS110 (CHB), PRO 218 (2 PAL), TYR 48, and LYS21 (CH). It was found to have two similar amino acid interactions (TYR-48, HIS-110) as that of the ligand tolrestat. Vijayoside was further considered for the MDS study.

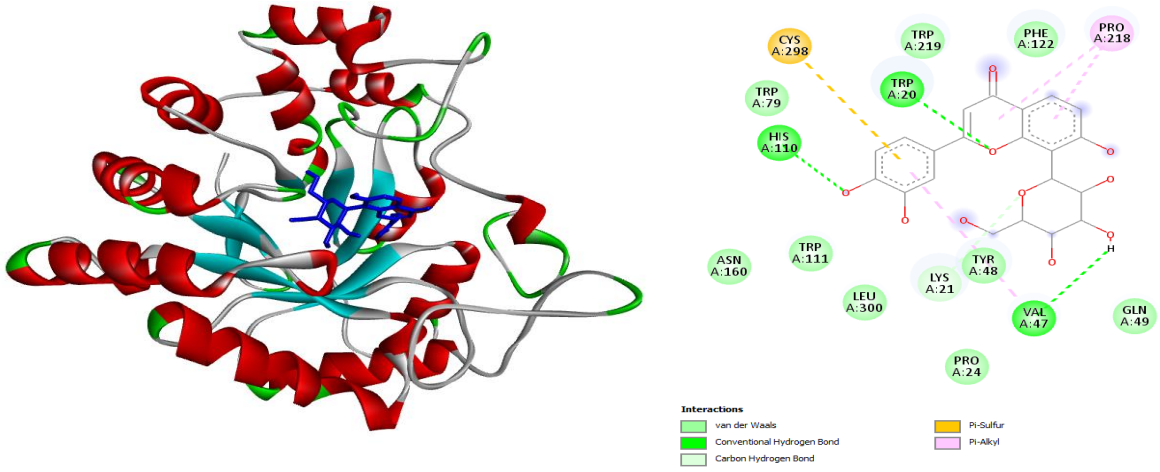

(a) **(b)**

Figure 4. Docked pose of **(a)**Vijayoside (blue) in the binding pocket of Aldose reductase (2FZD); **(b)** Interaction with Vijayoside.

3.2. Pharmacological properties of the ligands.

Lipinski's Rule of 5 (RO5) was followed to check the druggability of natural compounds [35]. If two or more rules are violated, the usefulness of the candidate as a drug is questionable. As shown in Table 3, RIF was found to comply with RO5, while Vijayoside and Pteroside each showed one violation. As per Veber's rule, the rotatable bond count was found to be less than or equal to 10, and the hydrogen bond acceptors and donors were less than or equal to 12. This study indicates good oral bioavailability of all compounds.

3.3. Molecular dynamics simulation analysis.

The molecular dynamics results confirmed stable behavior across all four protein–ligand complexes. RMSD analysis (Figure 5) showed fast equilibration followed by stabilized trajectories. The 2FZD_VIJ complex stabilized around ~1.1–1.8 Å with minor late-phase adjustments, while 4CFE_RIF exhibited higher deviation (~11–14 Å), indicating larger structural rearrangement but eventual convergence. The 4FFW_RIF complex fluctuated in a narrow window (~2–3 Å) and remained structurally stable. Similarly, 7VSI_PSD maintained a controlled RMSD (~2.5–3.0 Å) with no abrupt shifts, confirming steady binding throughout the simulation.

RMSF profiles (Figure 6) showed limited flexibility in most structural regions. All complexes exhibited higher mobility in loop or terminal segments, especially near residues ~225 in 2FZD_VIJ, ~280–320 in 4CFE_RIF, ~225 in 4FFW_RIF, and ~230 in 7VSI_PSD. Core structural elements remained stable with minimal fluctuation.

Rg (Figure 7) trends further supported global structural stability. 2FZD_VIJ maintained a compact fold, 4CFE_RIF showed moderate variability but no instability, 4FFW_RIF displayed gradual compaction, and 7VSI_PSD formed a tighter conformation in the later simulation stages.

Hydrogen-bond profiles (Figure 8) differed among complexes. The strongest and most consistent network was observed in 7VSI_PSD, whereas 4CFE_RIF formed fewer, less persistent interactions. The remaining two systems showed moderate yet stable H-bond formation.

SASA analysis (Figure 9) demonstrated reduced solvent exposure in all systems, indicating ligand-induced compaction. The largest reduction occurred in 2FZD_VIJ and 7VSI_PSD, confirming strong stabilizing effects upon ligand binding.

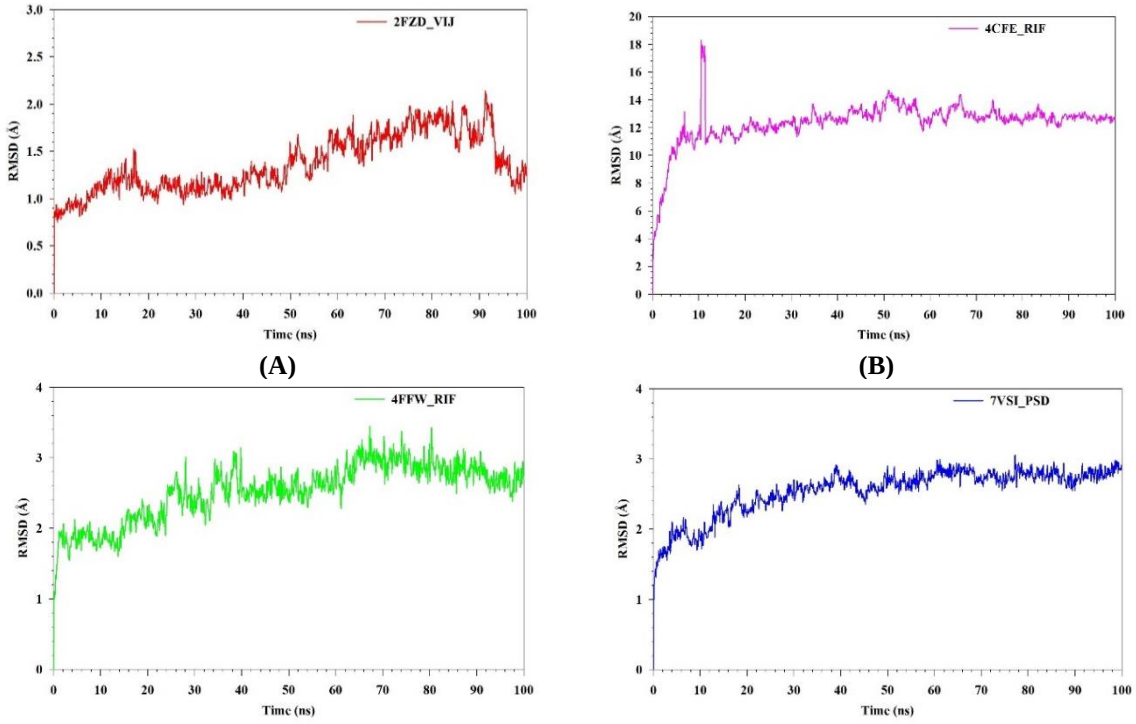

Figure 5. MD simulation analysis of 100 ns trajectories of RMSD of Cα backbone of (**A)** 2FZD_VIJ; **(B)** 4CFE_RIF; **(C)** 4FFW_RIF; **(D)** 7VSI_PSD.

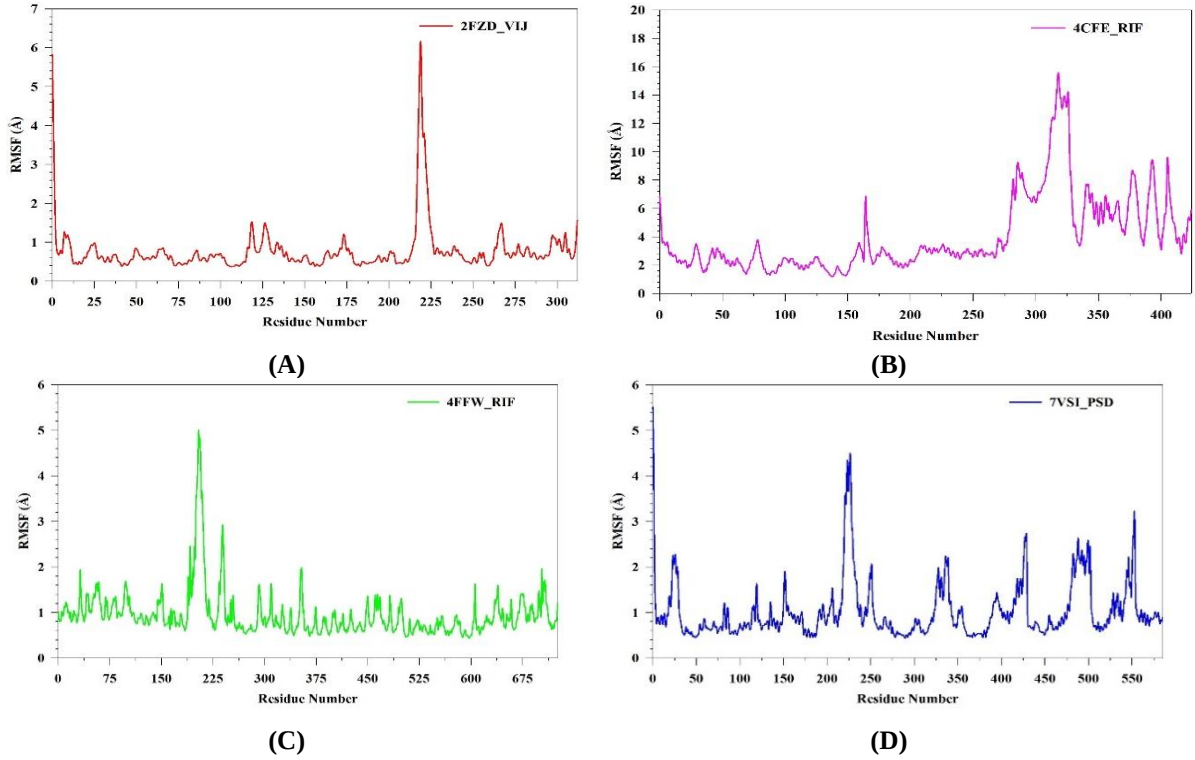

Figure 6. MD simulation analysis of 100 ns trajectories of RMSF of Cα backbone of **(A)** 2FZD_VIJ; **(B)**4CFE_RIF; **(C)** 4FFW_RIF; **(D)** 7VSI_PSD.

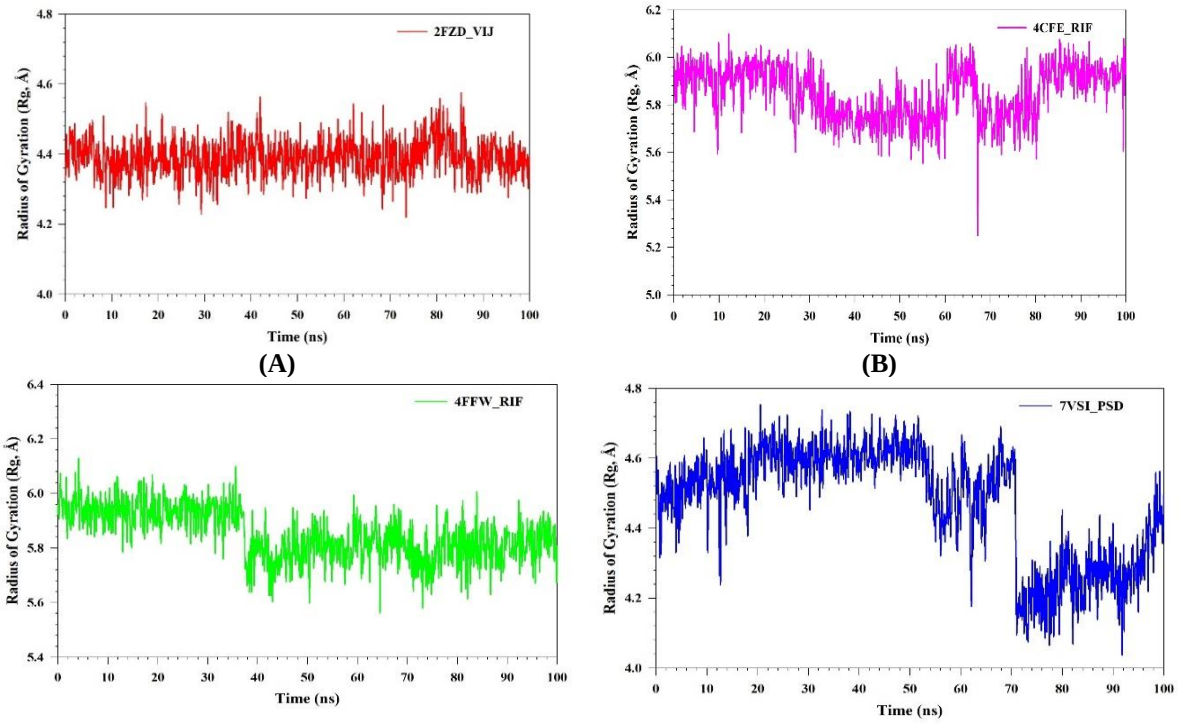

Figure 7. MD simulation analysis of 100 ns trajectories of Radius of Gyration (Rg) of Cα backbone of **(A)** 2FZD_VIJ; **(B)** 4CFE_RIF; **(C)** 4FFW_RIF; **(D)** 7VSI_PSD.

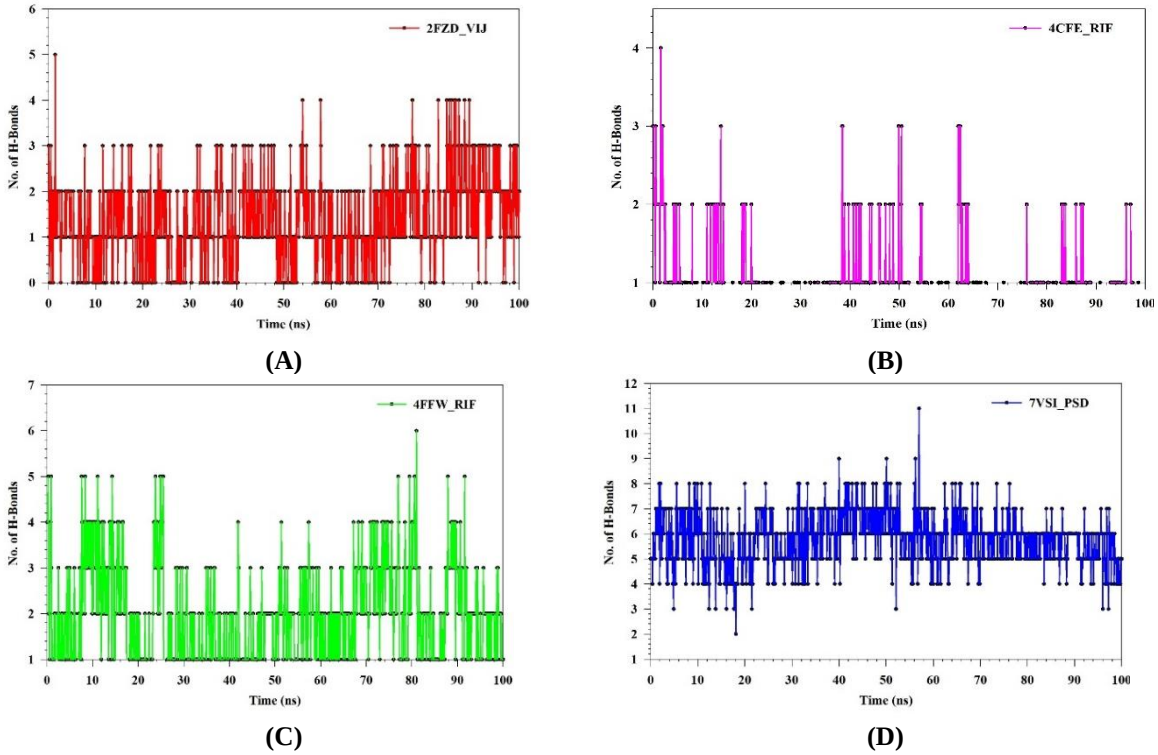

Figure 8. MD simulation analysis of 100 ns trajectories of Formation of hydrogen bonds in **(A)** 2FZD_VIJ; **(B)** 4CFE_RIF; **(C)** 4FFW_RIF; **(D)** 7VSI_PSD.

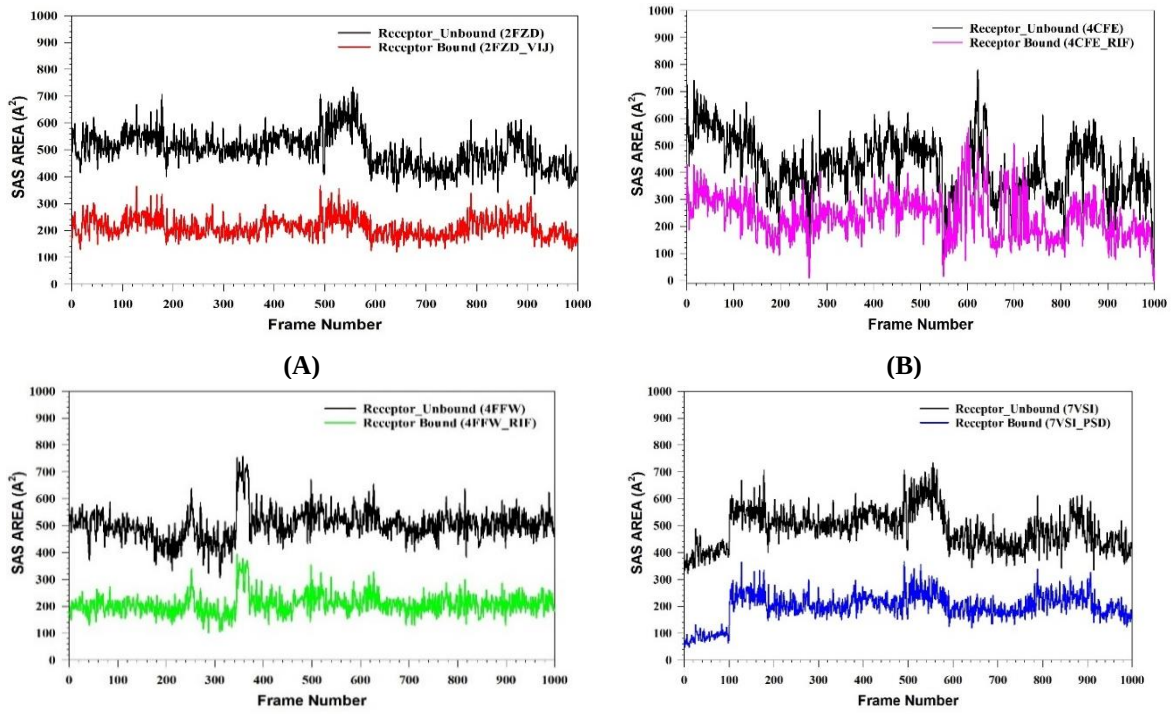

Figure 9. MD simulation analysis of 1000 Framework of Solvent accessible surface area of **(A)** 2FZD_VIJ; **(B)** 4CFE_RIF; **(C)** 4FFW_RIF; **(D)** 7VSI_PSD.

3.4. Molecular mechanics generalized born surface area (MM-GBSA) calculations.

MM-GBSA energy evaluation from the simulation trajectories revealed clear differences in binding strength among the four complexes. The 7VSI_PSD system exhibited the most favorable interaction energy (−58.94 kcal/mol), supported mainly by strong van der Waals and electrostatic contributions, alongside notable lipophilic and hydrogen-bond components. Despite a high solvation penalty, the net binding remained highly favorable, indicating a well-stabilized ligand pose.

The 4FFW_RIF complex showed the next strongest affinity (−51.58 kcal/mol), with stability driven by substantial nonpolar and electrostatic interactions. Although desolvation costs partially opposed binding, the overall energy profile confirmed stable ligand accommodation.

The 2FZD_VIJ complex demonstrated moderate binding strength (−38.20 kcal/mol). Here, hydrophobic and van der Waals terms dominated, while electrostatic and hydrogen-bond contributions were present but less pronounced. The solvation cost reduced the overall interaction strength but did not compromise stability.

Table 5. Binding free energy components for the 2FZD_VIJ, 4CFE_RIF, 4FFW_RIF, 7VSI_PSD complexes calculated by MM-GBSA.

Energies (kcal/mol)	2FZD_VIJ	4CFE_RIF	4FFW_RIF	7VSI_PSD
ΔG_{bind}	-38.20±2.69	-19.36±8.82	-51.58±6.82	-58.94±4.44
ΔG_{bind}Coulomb	-14.95±4.18	-4.01±4.64	-27.95±7.46	-33.41±3.55
ΔG_{bind}Covalent	0.76±0.46	0.45±0.49	2.32±2.38	4.62±1.07
$\Delta G_{bind}H_{bond}$	-1.12±0.25	-0.34±0.50	-1.70±0.37	-3.64±0.35
ΔG_{bind}Lipo	-17.43±0.47	-5.69±2.56	-12.69±0.35	-17.67±1.05
ΔG_{bind}Packing	-0.95±0.54	-1.40±1.61	-8.38±0.59	-4.65±0.63
ΔG_{bind}SolvGB	25.00±3.09	9.61±5.81	31.94±2.49	46.46±3.36
ΔG_{bind}VdW	-29.52±1.03	-18.00±7.58	-35.13±1.03	-50.65±2.30

Among all systems, 4CFE_RIF showed the weakest affinity (−19.36 kcal/mol), reflecting limited stabilizing interactions. Both polar and nonpolar contributions were

comparatively low, indicating fewer favorable contacts and a less firmly bound ligand state. The results are shown in Table 5.

Limitations of the study: This study is based on a computational approach and lacks experimental investigation.

4. Conclusions

Molecular docking has revealed that RIF has favorable binding affinities for DPP-4 and AMPK compared to the cocrystallized ligands Sitagliptin and benzimidazole. Similarly, Pteroside and Vijayoside bind stably with SGLT-2 and AR, respectively. Although more research focuses on the use of Pterostilbene in the management of DM, attention should also be given to investigating the roles of other phytoconstituents. Predicted pharmacokinetics and toxicity using the SwissADME server showed that Pteroside, Vijayoside, and RIF have good drug-likeness. The integrated molecular dynamics and MM-GBSA analysis confirmed differential stability and binding efficiency among the studied complexes. All systems remained structurally stable throughout the simulation. Among the evaluated complexes, Pteroside consistently demonstrated the strongest interaction profile with sodium glucose cotransporter-2, supported by the highest number of hydrogen bonds, a compact structural behavior, reduced solvent exposure, and the most favorable binding free energy. The dipeptidyl peptidase-4 with 7-O-α-L-rhamnopyranosyloxy-4′-methoxy-5-hydroxy isoflavone complex ranked second, showing stable conformational behavior and strong nonpolar and electrostatic contributions. Further, the efficacy of these phytocompounds may be proven with experimental studies.

Author Contributions

Conceptualization, R.P. and V.C.; methodology, R.P. and V.C.; software, S.T. and A.M.; validation, S.T., A.M., and V.T.; formal analysis, S.T. and A.M.; investigation, V.T.; resources, S.T. and A.M.; data curation, R.P. and V.C.; writing—original draft preparation, R.P. and V.C.; writing—review and editing, R.P. and V.T.; visualization, V.T.; supervision, V.C.; project administration, V.C. All authors have read and agreed to the published version of the manuscript.

Institutional Review Board Statement

Not applicable.

Informed Consent Statement

Not applicable.

Data Availability Statement

Data supporting the findings of this study are available upon reasonable request from the corresponding author.

Funding

This research received no external funding.

Acknowledgments

The authors are thankful to the School of Health Sciences and Technology, Dr. Vishwanath Karad, MIT World Peace University, and Progressive Education Society's Modern College of Pharmacy, Moshi, for their necessary support.

Conflicts of Interest

The authors declare no conflict of interest.

References

1. Macalalad, M.A.B.; Gonzales III, A.A. In-silico screening and identification of phytochemicals from *Centella asiatica* as potential inhibitors of sodium-glucose co-transporter 2 for treating diabetes. *J. Biomol. Struct. Dyn.* **2022**, *40*, 12221-12238, http://doi.org/10.1080/07391102.2021.1969282.
2. Yen, F.-S.; Wei, J.C.-C.; Yu, T.-S.; Hung, Y.-T.; Hsu, C.-C.; Hwu, C.-M. Sodium-Glucose Cotransporter 2 Inhibitors and Risk of Retinopathy in Patients With Type 2 Diabetes. *JAMA Netw. Open* **2023**, *6*, e2348431-e2348431, http://doi.org/10.1001/jamanetworkopen.2023.48431.
3. Singh, A.; Mishra, A. Molecular dynamics simulation and free energy calculation studies of Coagulin L as dipeptidyl peptidase-4 inhibitor. *J. Biomol. Struct. Dyn.* **2022,** *40*, 1128–1138, http://doi.org/10.1080/07391102.2020.1822917.
4. Saini, K.; Sharma, S.; Khan, Y. DPP-4 inhibitors for treating T2DM - hype or hope? an analysis based on the current literature. *Front. Mol. Biosci.* **2023**, *10*, 1130625, https://doi.org/10.3389/fmolb.2023.1130625.
5. Kitisripanya, T.; Buraphaka, H.; Boonsnongcheep, P.; Sritularak, B.; Likhitwitayawuid, K.; Putalun, W. Oxyresveratrol and its synthetic derivatives on the stimulation of glucose uptake in skeletal muscle cells and the activation of AMPK. *ScienceAsia* **2021**, *47*, 727–732, http://doi.org/10.2306/scienceasia1513-1874.2021.107.
6. Dutta, S.; Shah, R.B.; Singhal, S.; Dutta, S.B.; Bansal, S.; Sinha, S.; Haque, M. Metformin: a review of potential mechanism and therapeutic utility beyond diabetes. *Drug Des. Dev. Ther.* **2023**, *17*, 1907-1932, https://doi.org/10.2147/dddt.s409373.
7. Jannapureddy, S.; Sharma, M.; Yepuri, G.; Schmidt, A.M.; Ramasamy, R. Aldose Reductase: An Emerging Target for Development of Interventions for Diabetic Cardiovascular Complications. *Front. Endocrinol.* **2021**, *12*, 636267, https://doi.org/10.3389/fendo.2021.636267.
8. Singh, M.; Kapoor, A.; Bhatnagar, A. Physiological and Pathological Roles of Aldose Reductase. *Metabolites* **2021**, *11*, 655, https://doi.org/10.3390/metabo11100655.
9. Patil, R.; Aswar, U.; Vyas, N. Pterostilbene ameliorates type-2 diabetes mellitus – Induced depressive-like behavior by mitigating insulin resistance, inflammation and ameliorating HPA axis dysfunction in rat brain. *Brain Res.* **2023**, *15*, 148494, https://doi.org/10.1016/j.brainres.2023.148494.
10. Zhang, Y.; Ren, S.; Ji, Y.; Liang, Y. Pterostilbene Ameliorates Nephropathy Injury in Streptozotocin-Induced Diabetic Rats. *Pharmacology* **2019**, *104*, 71-80, http://doi.org/10.1159/000500293.
11. Dodda, D.; Ciddi, V. Pterostilbene alleviates diabetic nephropathy in experimental diabetic rats; inhibition of aldose reductase and advanced glycation end products formation. *Orient. Pharm. Exp. Med.* **2015**, *15*, 297-303, http://dx.doi.org/10.1007/s13596-015-0204-8.
12. Shen, H.; Rong, H. Pterostilbene impact on retinal endothelial cells under high glucose environment. *Int. J. Clin. Exp. Pathol.* **2015**, *8*, 12589-12594.
13. Mishra, A.; Srivastava, R.; Srivastava, S.P.; Gautam, S.; Tamrakar, A.K.; Maurya, R.; Srivastava, A.K. Antidiabetic activity of heart wood of Pterocarpus marsupium Roxb. and analysis of phytoconstituents. *Indian J. Exp. Biol.* **2013**, *51*, 363-374.
14. Ahmad, F.; Khan, M.M.; Rastogi, A.K.; Chaubey, M.; Kidwai, J.R. Effect of (-)epicatechin on cAMP content, insulin release and conversion of proinsulin to insulin in immature and mature rat islets in vitro. *Indian J. Exp. Biol.* **1991**, *29*, 516-520.
15. IMPPAT: Indian Medicinal Plants, Phytochemistry and Therapeutic. Available online: https://cb.imsc.res.in/imppat/, (accessed on 13th March 2024).

16. Mohanraj, K.; Karthikeyan, B.S.; Vivek-Ananth, R.P.; Chand, R.P.B.; Aparna, S.R.; Mangalapandi, P.; Samal, A. IMPPAT: A curated database of Indian Medicinal Plants, Phytochemistry and Therapeutics. *Sci. Rep*. **2018**, *8*, 4329, https://doi.org/10.1038/s41598-018-22631-z.
17. Perera, H.K.I. Antidiabetic Effects of Pterocarpus marsupium (Gammalu). *Eur. J. Med. Plants* **2016**, *13*, 1-14, https://doi.org/10.9734/EJMP/2016/23930.
18. Satheesh, M.A.; Pari, L. The antioxidant role of pterostilbene in streptozotocin-nicotinamide-induced type 2 diabetes mellitus in Wistar rats†. *J. Pharm. Pharmacol.* **2006**, *58*, 1483-1490, https://doi.org/10.1211/jpp.58.11.0009.
19. Anandharajan, R.; Pathmanathan, K.; Shankernarayanan, N.P.; Vishwakarma, R.A.; Balakrishnan, A. Upregulation of Glut-4 and PPARγ by an isoflavone from *Pterocarpus marsupium* on L6 myotubes: a possible mechanism of action. *J. Ethnopharmacol.* **2005**, *97*, 253-260, https://doi.org/10.1016/j.jep.2004.11.023.
20. Milton-Laskíbar, I.; Gómez-Zorita, S.; Arias, N.; Romo-Miguel, N.; González, M.; Fernández-Quintela, A.; Portillo, M.P. Effects of resveratrol and its derivative pterostilbene on brown adipose tissue thermogenic activation and on white adipose tissue browning process. *J. Physiol. Biochem.* **2020**, *76*, 269-278, https://doi.org/10.1007/s13105-020-00735-3.
21. Singh, P.; Bajpai, V.; Gupta, A.; Gaikwad, A.N.; Maurya, R.; Kumar, B. Identification and quantification of secondary metabolites of *Pterocarpus marsupium* by LC–MS techniques and its *in-vitro* lipid lowering activity. *Ind. Crops Prod.* **2019**, *127*, 26-35, https://doi.org/10.1016/j.indcrop.2018.10.047.
22. PubChem. National Center for Biotechnology Information; Bethesda, MD: 2004. Available at: https://pubchem.ncbi.nlm.nih.gov (accessed on 10th May 2024).
23. Avogadro: An Open-Source Molecular Builder and Visualization Tool. Version 1.2.0. Available online: http://avogadro.cc (accessed on 10th May 2024).
24. Hanwell, M.D.; Curtis, D.E.; Lonie, D.C.; Vandermeersch, T.; Zurek, E.; Hutchison, G.R. Avogadro: an advanced semantic chemical editor, visualization, and analysis platform. *J. Cheminform.* **2012**, *4*, 17, https://doi.org/10.1186/1758-2946-4-17.
25. Eberhardt, J.; Santos-Martins, D.; Tillack, A.F.; Forli, S. AutoDock Vina 1.2.0: New Docking Methods, Expanded Force Field, and Python Bindings. *J. Chem. Inf. Model.* **2021**, *61*, 3891-3898, https://doi.org/10.1021/acs.jcim.1c00203.
26. Niu, Y.; Liu, R.; Guan, C.; Zhang, Y.; Chen, Z.; Hoerer, S.; Nar, H.; Chen, L. Structural basis of inhibition of the human SGLT2–MAP17 glucose transporter. *Nature* **2022**, *601*, 280-284, https://doi.org/10.1038/s41586-021-04212-9.
27. Tang, J.; Majeti, J.; Sudom, A.; Xiong, Y.; Lu, M.; Liu, Q.; Higbee, J.; Zhang, Y.; Wang, Y.; Wang, W.; Cao, P.; Xia, Z.; Johnstone, S.; Min, X.; Yang, X.; Shao, H.; Yu, T.; Sharkov, N.; Walker, N.; Tu, H.; Shen, W.; Wang, Z. An Inhibitory Antibody against Dipeptidyl Peptidase IV Improves Glucose Tolerance *in Vivo*. *J. Biol. Chem.* **2013**, *288*, 1307-1316, https://doi.org/10.1074/jbc.M112.396317.
28. Xiao, B.; Sanders, M.J.; Carmena, D.; Bright, N.J.; Haire, L.F.; Underwood, E.; Patel, B.R.; Heath, R.B.; Walker, P.A.; Hallen, S.; Giordanetto, F.; Martin, S.R.; Carling, D.; Gamblin, S.J. Structural basis of AMPK regulation by small molecule activators. *Nat. Commun.* **2013**, *4*, 3017, https://doi.org/10.1038/ncomms4017.
29. Steuber, H.; Zentgraf, M.; Gerlach, C.; Sotriffer, C.A.; Heine, A.; Klebe, G. Expect the Unexpected or Caveat for Drug Designers: Multiple Structure Determinations Using Aldose Reductase Crystals Treated under Varying Soaking and Co-crystallisation Conditions. *J. Mol. Biol.* **2006**, *363*, 174-187, https://doi.org/10.1016/j.jmb.2006.08.011.
30. Dallakyan, S.; Olson, A.J. Small-Molecule Library Screening by Docking with PyRx. In Chemical Biology: Methods and Protocols, Hempel, J.E., Williams, C.H., Hong, C.C., Eds.; Springer New York: New York, NY, **2015**; Volume 1263, pp. 243-250, https://doi.org/10.1007/978-1-4939-2269-7_19.
31. Daina, A.; Michielin, O.; Zoete, V. SwissADME: a free web tool to evaluate pharmacokinetics, drug-likeness and medicinal chemistry friendliness of small molecules. *Sci. Rep.* **2017**, *7*, 42717, https://doi.org/10.1038/srep42717.
32. Rafiq, A.; Tayyab, M.; Mali, S.N.; Taslimi, P.; Jawarkar, R.D.; Gurav, S.S.; Zhao, X.; Sadeghian, N.; Çakır, F.; Shafiq, Z.; Tawfeek, A.M.; Shahidul Islam, M. Synthesis, human carbonic anhydrase I and II inhibition, and in silico studies of 2-ethoxy-6-formylphenyl [1,1′-biphenyl]-4-sulfonate derived thiosemicarbazones. *Bioorg. Chem.* **2025**, *164*, 108836, https://doi.org/10.1016/j.bioorg.2025.108836.

33. Kuştan, F.; Sıcak, Y.; Mali, S.N.; Chaudhari, S.Y.; Öztürk, M.; Tok, F. Synthesis, biological evaluation, molecular docking and MD simulation studies of some new picolinohydrazide derivatives as cholinesterase inhibitors. *J. Mol. Struct.* **2026**, *1349*, 143637, https://doi.org/10.1016/j.molstruc.2025.143637.
34. Bakal, R.L.; Jawarkar, R.D.; Manwar, J.V.; Jaiswal, M.S.; Ghosh, A.; Gandhi, A.; Zaki, M.E.A.; Al-Hussain, S.; Samad, A.; Masand, V.H.; Mukerjee, N.; Nasir Abbas Bukhari, S.; Sharma, P.; Lewaa, I. Identification of potent aldose reductase inhibitors as antidiabetic (Anti-hyperglycemic) agents using QSAR based virtual Screening, molecular Docking, MD simulation and MMGBSA approaches. *Saudi Pharm. J.* **2022**, *30*, 693-710, https://doi.org/10.1016/j.jsps.2022.04.003.
35. Kralj, S.; Jukič, M.; Bren, U. Molecular Filters in Medicinal Chemistry. *Encyclopedia* **2023**, *3*, 501-511, https://doi.org/10.3390/encyclopedia3020035.

Publisher's Note & Disclaimer